In Vivo Cancer Cells Elimination Guided by Aptamer-Functionalized Gold-Coated Magnetic Nanoparticles and Controlled with Low Frequency Alternating Magnetic Field

Irina V. Belyanina[2,3], Tatiana N. Zamay[2,3], Galina S. Zamay[1,2], Sergey S. Zamay[1], Olga S. Kolovskaya[1,2], Tatiana I. Ivanchenko[2], Valery V. Denisenko[5,3], Andrey K. Kirichenko[2], Yury E. Glazyrin[2], Irina V. Garanzha[2,3], Valentina V. Grigorieva[2,3], Alexandr Shabanov[1], Dmitry V. Veprintsev[1,2], Alexey E. Sokolov[1,3], Vladimir M. Sadovskii[5,3], Ana Gargaun[4], Maxim V. Berezovski[4], Anna S. Kichkailo[1,2]

[1]*Federal Research Center, KSC Siberian branch of Russian Academy of Science, Krasnoyarsk, Russia*

[2]*Krasnoyarsk State Medical University named after Professor V. F. Voyno-Yasenetsky, Krasnoyarsk, Russia*

[3]*Siberian Federal University, Krasnoyarsk, Russia*

[4]*University of Ottawa, Department of Chemistry and Biomolecular Sciences, Ottawa, Ontario Canada*

[5]*Institute of Computational Modeling RAS SB, Krasnoyarsk, Russia*

Corresponding authors: Anna S. Kichkailo, azamay@krasgmu.ru

Abstract

Biomedical applications of magnetic nanoparticles in a magnetic field have exceeded many expectations in cancer therapy. Magnetic nanoparticles are effective heat mediators, drug nanocarriers, and contrast agents; various strategies have been suggested to selectively target tumor cancer cells but not healthy cells. Our study presents magnetodynamic nanotherapy utilizing DNA aptamer-functionalized 50 nm gold-coated magnetic nanoparticles exposed to a low frequency alternating magnetic field for precise elimination of tumor cells *in vivo*. The cell specific DNA aptamer AS-14 binds to fibronectin protein in Ehrlich carcinoma and delivers gold-coated magnetic nanoparticles to a mouse tumor. An alternating magnetic field of 50 Hz causesthe nanoparticles to oscillate and pull fibronectin and integrins on the surface of the cell membrane resulting in massive cell apoptosis followed by necrosis without heating the tumor, adjacent healthy cells and tissues. The aptamer-guided nanoparticles and the low frequency alternating magnetic field demonstrates a unique technology of a non-invasive nanoscalpel for precise cancer surgery at a single cell level.

Keywords: cancer therapy; gold coated magnetic nanoparticles; DNA aptamers; low frequency alternating magnetic field, fibronectin, integrin, apoptosis, necrosis.

Introduction

Medical nanotechnologies are becoming promising for cancer treatment. A variety of nanomaterials and nanoparticles (NPs) have been synthesized for diagnostic and therapeutic applications [1, 2]. At the nanometer scale, materials exhibit novel optical, magnetic, electronic, and structural properties [1, 3], which make nano-sized particles promising in molecular diagnostics and anti-cancer therapy [4]. Magnetic nanoparticles (MNPs) can be used as effective heat mediators, drug carriers, and contrast agents [4, 5]. The main problem is that nanoparticles accumulate in healthy tissues causing harmful effects [6, 7]. Targeted delivery requires functionalization of nanoparticles with molecular probes such as antibodies or aptamers that bind specifically to unique or overexpressed biomolecules on cancer cells [7, 8]. Aptamers are short synthetic single-stranded DNA or RNA that specifically bind to various targets, such as inorganic ions, small organic molecules, peptides and proteins, whole cells and tissues with high affinity and selectivity [4, 5, 9]. Low immunogenicity, toxicity and cost make aptamers attractive for therapeutic applications [4].

Aptamer-functionalized nanoparticles have been utilized for cancer therapy including photodynamic therapy (PDT) [10] and photothermal therapy (PTT) [11, 12]. PDT is minimally invasive and minimally toxic. It destroys cells by reactive oxygen species generated with light and a photosensitizer. Conjugation of aptamers with nanoparticles improves accumulation of particles in tumor tissue and selective photo-induced damage during PDT. Similar to PDT, PTT is a fairly non-invasive cancer treatment. PTT is based on the ability of gold nanoparticles to absorb light and convert it into heat that promotes destruction of abnormal cells. The effectiveness of this method has been successfully demonstrated on mouse tumor remission [13]. Huang YF et al. demonstrated the use of aptamers conjugated to nanorods for targeted PTT of human leukemia [14].

Advantages of PDT and PTT include the less invasive nature of light-based therapies when compared to surgery and the ability to deliver irradiation with great accuracy as well as multiple times over at the same site. However, disadvantages of PDT and PTT include limited accessibility as they can only treat areas that can be reached by light (on or under the skin, or in the lining of organs that can be reached with a light source). Therefore, light-based therapies cannot be used to treat cancers that have grown deeply into the skin or other organs, or that have metastasized.

In this study, we demonstrate the utility of alternative magnetodynamic therapy to eradicate a tumor in mice (Figure 1). We applied aptamer-modified gold-coated magnetic nanoparticles (AGMNPs) to target a tumor *in vitro* and *in vivo*. For the selective targeting, we used aptamer AS-14 to mouse Ehrlich carcinoma fibronectin (Fn) described in our previous study [15]. Fn is a large adhesive glycoprotein protein, an essential component of the extracellular matrix, which assembles into fibrils, attaching cells to the collagen fibers. It has been shown that along with extracellular Fn, Ehrlich ascites cells synthesize and release large amounts of Fn into the culture medium *in vitro*, and into ascitic fluid and plasma *in vivo* [16]. Fn plays a major role in cell growth, differentiation, migration, wound healing, blood coagulation, embryonic development, and also in oncogenic transformation [17-19]. Fn shows higher expression and different distribution in breast carcinomas than in normal breast parenchyma. Its expression in cancer cell cytoplasm is associated with distant metastasis development and survival rate both in humans and mice [17].

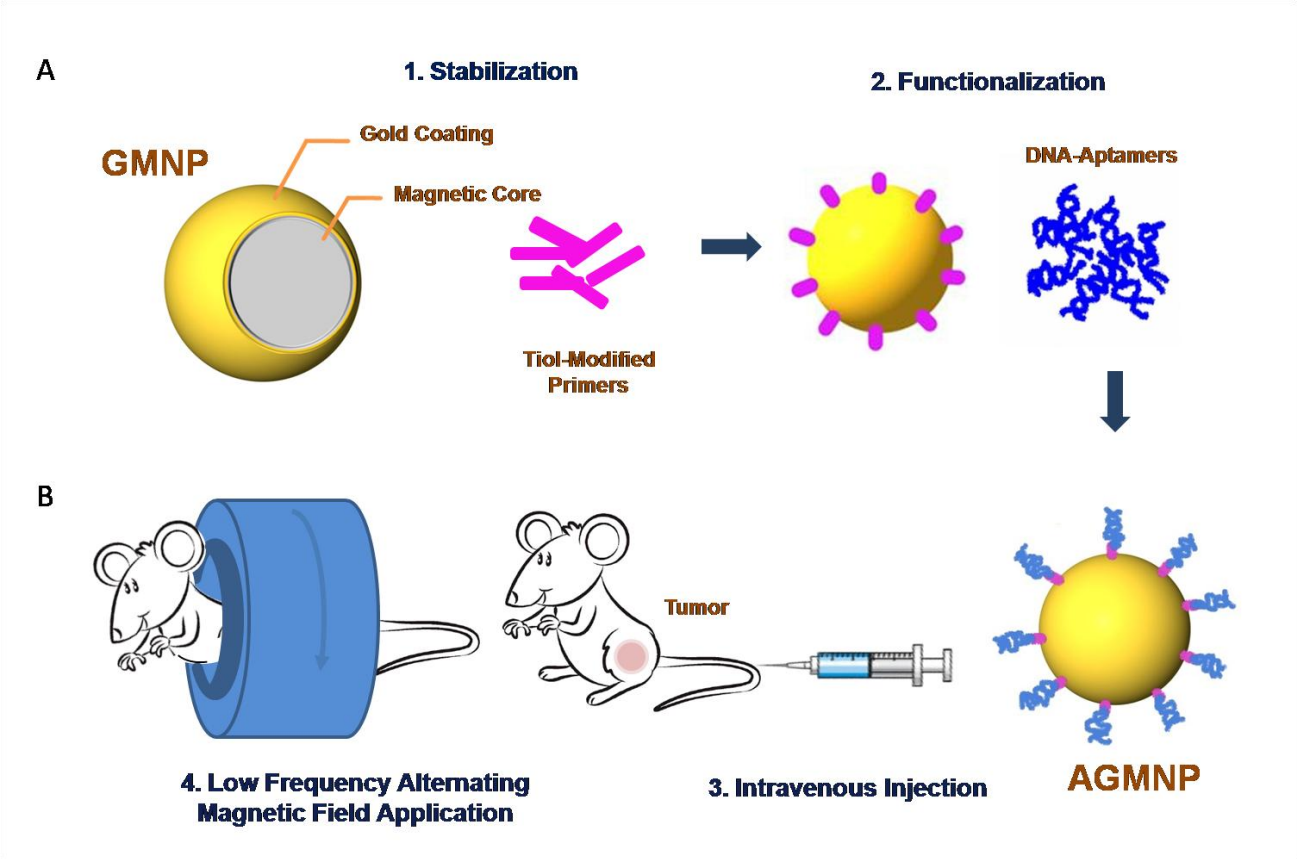

Figure 1. Schematic representation of the modification of gold-coated magnetic nanoparticles (GMNPs) with a thiolated oligonucleotide primer followed by hybridization with a cancer cell specific aptamer (A). Schematic representation of tumor magnetodynamic nanotherapy in a low frequency alternating magnetic field (B).

Aptamer AS-14 delivers GMNPs to Ehrlich carcinoma tumor and links the particles with fibronectin molecules. Fns bind to the cell surface via integrins - large trans membrane adhesion proteins that provide the physical link between the extracellular matrix and the contractile cytoskeleton [20]. Integrins and conventional signalling receptors often cooperate to promote cell growth, cell survival, and cell proliferation [21]. Integrin activation has a structural origin [22, 23], once a ligand binds to it, its head opens the hinge between the β-subunit and hybrid headpiece domain and a mechanical force greatly accelerates the hinge opening [24-26]. Recently reported experimental data and molecular design simulations demonstrate the dynamics of integrin activation due to ligand binding and a mechanical force pulling integrin to 6 nm for 6 ns[24]. Integrin-mediated apoptosis could be induced by its activation followed by direct recruitment and activation of caspase-8 [21, 27-32]. The low frequency alternating magnetic field (LFAMF) causes oscillations of GMNPs and the complex of the aptamers with fibronectin. Therefore, activity of NPs was modulated by LFAMF. The advantages of the proposed technology are the deep penetration of a magnetic field, high cytotoxic activity toward cancer cells and low toxicity on adjacent cells and healthy tissues.

Materials and Methods

Ethics Statement

This study was carried out in strict accordance with the recommendations in the Guide for the Care and Use of Laboratory Animals of the National Institute of Health. The protocol was approved by the Local Committee on the Ethics of Animal Experiments of the Krasnoyarsk State Medical University. All procedures were performed under anesthesia and all efforts were made to minimize suffering of the animals.

Mouse Tumor Model

White 6-week-old 25 g Imprinting Control Region (ICR) mice were provided by Siberian Federal University. Two million Ehrlich ascites carcinoma cells were transplanted into the right leg of each mouse. On days 5, 7 and 9 after the tumor transplantation, all animals were treated using aptamer AS-14 functionalized gold-coated magnetic nanoparticles in low frequency alternating magnetic field. For the *in vitro* studies Ehrlich ascites carcinoma cell cultures were utilized. Mouse ascites cells were cultured in 35×10 mm cell culture dishes (CELLSTAR®, Germany) in Dulbecco's modified Eagle's medium (DMEM; Sigma-Aldrich), supplemented with 100 UmL^{-1} penicillin, 100 UmL^{-1} streptomycin, and 5% (v/v) fetal bovine serum (FBS) in a humidified atmosphere containing 5% CO_2 at 37°C. All cell experiments were performed in DPBS containing 0.9 mM $CaCl_2$ and 0.49 mM $MgCl_2$.

Low frequency magnetic field induction

The magnetic coil was specially designed for the magnetodynamic experiments: the copper wire (0.53 mm in diameter) was wound on a cylinder with an inner diameter of 28 mm; the external diameter of the coil was 80 mm, and the resistance of the coil was 21.4 Ω. The coil creates a sinusoidal magnetic field of 100 Oe at a frequency of 50 Hz. The power dissipated in the coil was approximately 1.7 W, which did not heat the coil and sample of cells or the inside of the animal during the procedure. After each treatment, the coil was switched off for 10 minutes in order to avoid the possibility of heating.

Functionalization of Gold-Coated Magnetic Nanoparticles with DNA Aptamers

Gold-coated magnetic nanoparticles (GMNPs) were used with a diameter of 50nm, with a magnetic core of 8-12 nm and a golden shell of 30-40 nm (NITmagoldCit 50nm, Nanoimmunotech, Spain), (Supporting information, Figure S1). Nanoparticles stabilization was carried out with an HPLC purified oligonucleotide complimentary to the 5' of aptamer 5′-CGT GGTTACAGTCAGAGGAGAA-/5ThioMC6-D/-3′ modified at the 3′ position with a 6-hydroxyhexyl disulfide group (Integrated DNA Technologies, USA), in the GMNPs storage buffer for 24 hours at 4°C in a shaker (final concentration of 500nM). This mixture was diluted twice by mixing it with 2×DPBS (with calcium and magnesium) and mixed 1:1 with an equimolar amount of AS-14 aptamer (5′-TCCTCTGACTGTAACCACGAAGGTGTCGGCCTTAGTAAGGCTACAGCCAAGGGAAC GTAGCATAGGTAGTCCAGAAGCC-3′), which was previously heated at 95°C for 10 minutes and cooled on ice for 10 minutes, then incubated for an additional 24 hours at 4°C while shaking (Figure 1A).

Optimization of treatment conditions for magnetodynamic nanotherapy *in vitro*.

One million ascites Ehrlich carcinoma cells in 1 mL of colorless high glucose DMEM medium were incubated with AS-14-GMNPs or non-functionalized GMNPs at 1:25, 1:50, 1:75 or 1:100 ratios (final concentration 1×10^8 particles per 1 mL) or only DPBS with calcium and magnesium for 5, 15 or 30 minutes at 37°C in a humidified atmosphere containing 5% CO_2. All samples were prepared in triplicates. After incubation, the cells were washed twice with the same buffer and were kept in a magnet producing LFAMF for 1, 3, 5, 7 or 10 minutes. Cell viability was estimated 2 hours after the treatment (cells were captured at 37°C in a humidified atmosphere containing 5% CO_2) using propidium iodide dye (PI) (for timing the treatment procedure). Binding of GMNPs and viability were measured using flow cytometry (FC-500, Beckman Coulter, USA).

***In Vitro* Analyses of the Effects of AMNPs in a Low Frequency Alternating Magnetic Field**

Ehrlich carcinoma cells treated with AS-14-GMNPs or non-functionalized GMNPS at 1:100 ratios (final concentration 1×10^8 particles per 1 mL) or only DPBS 30 minutes at 37°C in

a humidified atmosphere containing 5% CO_2, washed and kept in a magnet producing LFAMF for 10 minutes. All samples were prepared in triplicates.

Apoptosis induction has been evaluated by caspase cascade activation in tumor cells, after 3 hours of treatment (cells were captured at 37°C in a humidified atmosphere containing 5% CO_2) using CellEvent™ Caspase-3/7 Detection Reagent (5μM in PBS with 5% FBS) (Thermo Fisher Scientific, USA) for 30 minutes at 37°C. The fluorescent signal from CellEvent Caspase-3/7 Detection Reagent has been detected using flow cytometry (FC-500, Beckman Coulter, USA). Inhibition of caspase cascade activation has been performed by concurrent binding of antibodies to mouse fibronectin prior the treatment. The cells were incubated in DPBS / 10% serum to block non-specific protein-protein interactions followed by the antibody (Anti-Fibronectin antibody [TV.1], Abcam, plc., USA,) at final concentration 0.7 μg/ml for 30 min at 37°C. The secondary antibody Donkey anti-rabbit IgG H&L Alexa Fluor® 647, Abcam, plc., USA) was used at 1/2000 dilution for 30 min at 37°C. Control antibody (Anti-Actin antibody [ACTN05 (C4)], Abcam, plc., USA) was used under the same conditions. Binding has been measured using flow cytometry (FC-500, Beckman Coulter, USA).

Apoptosis by Annexin V-Cy3 (Sigma Aldrich, USA), phosphatidylserine translocation, and 6-carboxyfluorescein diacetate (6-CFDA) (Sigma Aldrich, USA), which enters the cell and is hydrolyzed by esterases present in living cells to the fluorescent compound 6-carboxyfluorescein, indicating that the cells are viable (for cell death mechanisms identification). The procedures were done in accordance with the manufacturer's protocol and analysed using flow cytometry.

Intracellular sodium content was estimated with SBFI probe (Thermo Fisher Scientific, USA) by flow cytometry (FC-500, Beckman Coulter, USA) according to manufacturer's protocols.

***In Vivo* Antitumor Activity of Aptamer Modified GMNPs in LFAMF**

Six-week-old 25g ICR male mice were used in this study. For two weeks before the experiments, animals were trained to stay calm inside the magnetic coil. Two million Ehrlich's carcinoma cells were transplanted into the right leg of each mouse. Every second day, starting from day five after tumor transplantation until day nine, animals underwent10 minutes of magnetodynamic therapy in LFAMF with aptamer modified magnetic nanoparticles, free nanoparticles, free AS-14 or just DPBS (Figure 1B).

The mice were randomly administered tail vein injections (on days 5, 7 and 9 after the tumor transplantation, 3 times total) by dividing the mice into four groups with 7 animals in each group as follows:

Group 1: Injection of AS-14-GMNPs in 100 μL DPBS (1.6 μg kg^{-1});

Group 2: Injection of free GMNPs in 100 μL DPBS (1.6 μg kg^{-1});

Group 3: Injection of free AS-14 in 100 μL DPBS (0.4 mg kg^{-1});

Group 4: Injection of 100 μL DPBS.

After 30 minutes, animals were placed inside the magnet and were treated with a low frequency alternating magnetic field for 10 minutes.

Caspase Activity in Tumor Tissues

To evaluate apoptosis induction by caspase activity in tumor cells, after 3 hours of treatment a freshly harvested piece of a tumor was stained with CellEvent™ Caspase-3/7 (5μM in PBS with 5% FBS) (Thermo Fisher Scientific, USA) for 30 minutes at 37°C, washed with DPBS and fixed with 3.7% formalin. A series of 30μm tissue sections were prepared using cryostat HM 525 (Carl Zeiss, Germany) and fixed on glass slides and imaged with laser scanning microscope (Carl Zeiss LSM780, Germany).

Histological Analysis

To evaluate histological changes of the tumors after magnetodynamic therapy, microscopy of the tissue sections was performed (Axioskop 40, Carl Zeiss, Germany). Tumors were harvested and placed in 3.7% formalin. A series of 10 μm tissue sections were prepared using cryostat HM 525 (Carl Zeiss, Germany)andfixed on glass slides for hematoxylin and eosin staining.

AS-14-GMNPs Distribution in Tumor after Injection in Tail Vein

AS-14-GMNPs distribution in tumor and other organs after injection in the tail vein was analyzed using electron microscopy on 30μm tissue sections. On day 7 after the tumor transplantation, the mice were injected with GMNPs functionalized with FAM-labeled aptamer AS-14 in 100 μL DPBS (1.6 μg kg^{-1}). After 1, 5 and 24 hours the animals was euthanized and the tumor, liver, kidney and urine were harvested, 30μm tissue sections were prepared using cryostat HM 525 (Carl Zeiss, Germany), fixed on glass slides and placed on silicon foil. An electron microscopy (Hitachi TM3000, Japan) was used to visualize and estimate percentage ratios of iron and gold. EM spectra were processed with the software Quantax 70 (Bruker) for Hitachi TM3000.

Search of Protein Post-Translational Modifications

Search of protein post-translational modifications (PTM) was performed by Proteome Discoverer 1.4 software with Sequest HT search engine. The following seven variable modifications were set: oxidation, deamidation, phosphorylation, glycosylation, acetylation, methylation, acetylation (protein N-terminus). The search results were filtered and only modified peptides were selected. Values of peptide spectra matches (PSM) between modified and non-

modified peptides were considered as degrees of modification. Only peptides with prevalence in PSM for modified type or not presented as non-modified were selected as reliable.

***In Vivo* Toxicity Studies of Aptamer-Modified GMNPs in LFAMF**

Healthy six-week old 25g ICR mice were used in this study, 10 animals per group. The mice (5 female and 5 male in each group) were administered tail vein injections on days 1, 3 and 5 (3 times total) as follows:

Group 1: Injection of AS-14-GMNPs in 100 μL DPBS (1.6 μg kg^{-1});

Group 2:Injection of 100 μL DPBS.

Toxicity was estimated based on changes in blood biochemistry (cholesterol, total protein, alanine amino-transferase, alkaline phosphatase and bilirubin), which were performed using COBAS INTEGRA 400 plus analyzer (Roche Diagnostics, Switzerland). Male and female parameters were analyzed separately. All data were presented as the mean ± standard error of mean.

Results and Discussion

Our study demonstrates efficacy of targeted GMNPs-based magnetodynamic cancer cell disruption *in vitro* and *in vivo* in a low frequency alternating magnetic field. For the experiments, we used commercially available gold-coated magnetic nanoparticles with a diameter of 50 nm, a magnetic core of 8-12 nm and a 30-40 nm golden shell. Magnetic core of the particles provided magnetodynamic effects on cells, golden coating is used to attach aptamers to the surface through SH groups, moreover coating with gold make iron particles less toxic and increase their biocompatibility *in vivo*. The full description is presented in Supporting Information. The behaviour of aptamer-modified GMNPs in a magnetic field of alternating frequency in a colloid solution in DPBS at a concentration of 1×10^8 particles per 1 mL, which was suitable for the therapeutic purposes, was estimated using magnetic circular dichroism (MCD). At a frequency of 50 Hz, the MCD of the particles *in vitro* in sinusoidal magnetic field sufficiently increased and all particles magnetized (Figure S1).

Mathematical simulations showed that a sinusoidal magnetic field of 100 Oe at a frequency of 50 Hz induced magnetodynamic cell disruption with minimal possible thermal effects on cells and tissues (Supporting Information) therefore it could be used for magnetodynamic purposes. For selective targeting we used aptamer AS-14 to mouse Ehrlich carcinoma fibronectin (Fn) described in our previous study [15]. Here we revealed that Fn from Ehrlich carcinoma cells recognized by aptamer AS-14 has several post-translational modifications in 5 domains of Fn type III ($FnIII_5$): threonine is acetylated at the position 32 and phosphorylated at the position 36. These modifications are not currently described in the Protein

Data Bank http://www.rcsb.org/pdb/protein/P02751, therefore, suggesting that they are unique to mouse Ehrlich carcinoma cells. Potentially, aptamer AS-14 recognizes particularly this region, which is located between collagen binding and cell attachment sites.

Aptamer AS-14 delivers GMNPs to Ehrlich carcinoma tumor and links the particles with fibronectin molecules. The low frequency alternating magnetic field causes oscillations of the GMNPs in the complex with the aptamers bound to fibronectin. The mathematical modeling of the magneto-mechanical action of AS-14-GMNPs on cells is described in Supporting Information. Interestingly, LFAMF did not cause local hyperthermia (Supporting Information). LFAMF rotates a nanoparticle bound to $FnIII_5$ clockwise pulling the integrin β-subunit via $FnIII_{10}$ and returns it to its original position (Figure 2).

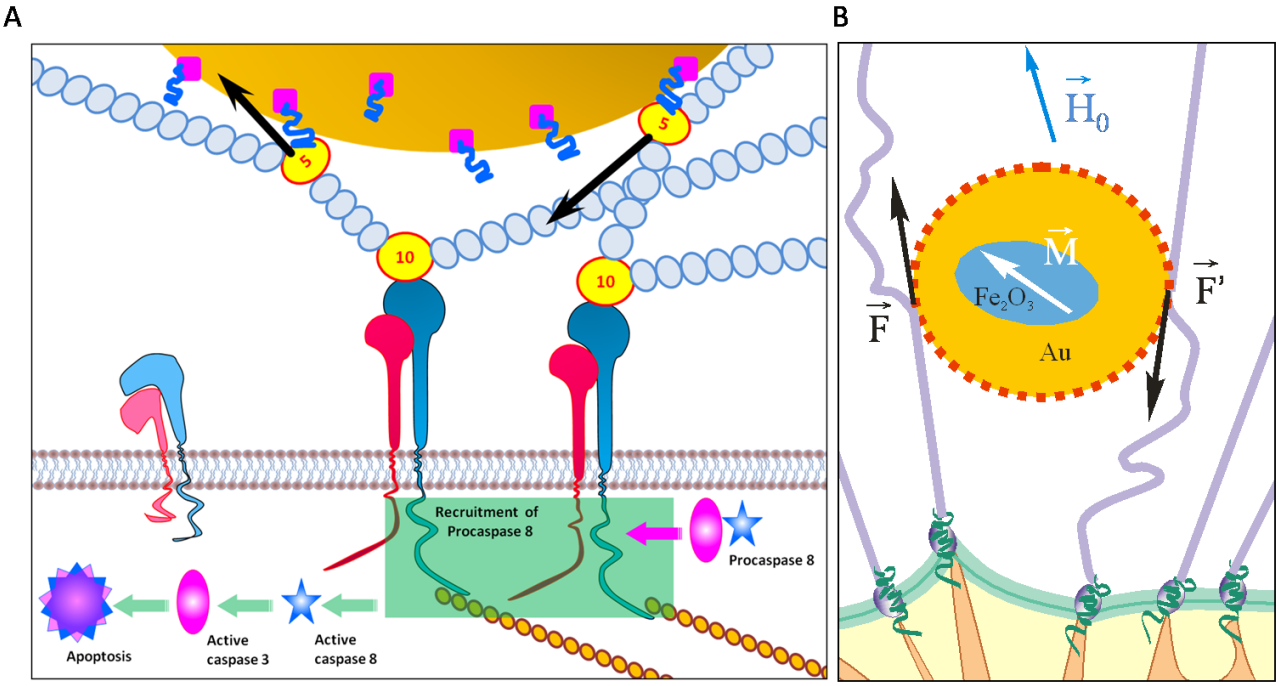

Figure 2. Schematic representation of an apoptotic caspase cascade. (A) The cascade is caused by fibronectin oscillation in a low frequency alternating magnetic field controlled by AS-14-GMNPs. (B) Forces applied to an AS-14-GMNP in the presence of a low frequency alternating magnetic field, where $\vec{F}$ – is the force pulling fibronectin; $\vec{M}$ – is magnetic moment of GMNP; and $\vec{H}_0$ –is an external magnetic field.

We calculated the magnetic moment, force and time of action of the magnetic particles in LFAMF (Supporting Information). LFAMF with a frequency of 50 Hz makes AS-14-GMPS periodically pull and relax the C terminus of $FnIII_{10}$ to 0.07 nm for 0.01 seconds, that means twice per period of LFAMF variation. Mechanical forcepulling of integrin activates FnIII [24] and causes integrin-mediated apoptosis by direct recruitment and activation of caspase-8 [21, 27-

32]. We think that oscillation of AS-14-GMNPscaused by LFAMF influences integrins via Fn and causes activation of caspases followed by cell apoptosis (Figure 2).

Effects of Aptamer-Modified GMNPs in LFAMF *In Vitro*

In order to optimize the therapeutic procedure *in vitro*, titration experiments at different incubation times have been performed. Incubation time did not influence binding much as after 5 minutes most cells appeared to be bound with aptamer modified fluorescently labelled nanoparticles, 75 and 100 particles bound per cell. Binding of 25 and 50 particles per cell required more time for efficient binding (Figure 3A).

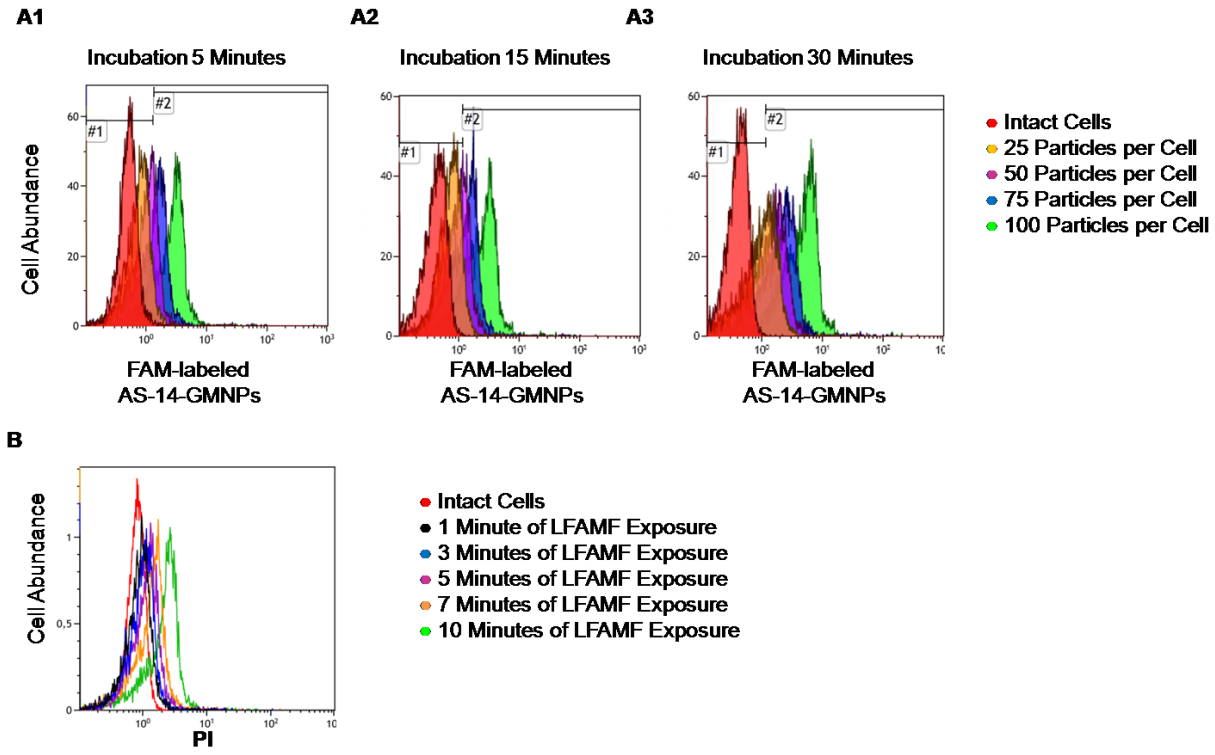

Figure 3. Optimization of treatment conditions for magnetodynamic nanotherapy *in vitro*. (A) Determination of the binding time for different amounts of AS-14 modified GMNPs per cell. Histograms of binding of 25 particles per cell (orange); 50 particles per cell (purple); 75 particles per cell (blue), and 100 particles per cell (green) after 5 minutes (A1); 15 minutes (A2), and 30 minutes of incubation (A3). (B) Viability of Ehrlich cells pre-incubated with AS-14-GMNPs (ratio of 100 particles per cell for 30 minutes) after 1, 3, 5, 7, and 10 minutes of LFAMF exposure.

One hundred particles per cell was enough to prompt binding, therefore this concentration was chosen for *in vitro* experiments and to insure all cells specifically bound with the particles incubation time was always 30 minutes. In order to adjust the time of LFAMF exposure, Ehrlich carcinoma cells bound with AS-14-GMNPs (a ratio of 1:100 particles after 30 minutes of

incubation) were placed in the center of the magnetic coil in LFAMF for 1, 3, 5, 7, and 10 minutes (Figure 3). The cellular death was registered in two hours after the treatment using propidium iodide (PI) dye by flow cytometry. Ten minutes were sufficient to induce Ehrlich carcinoma cells death and to avoid heating of the magnetic coil during this time.

In order to prove our suggestions that oscillations of AS-14-GMNPs bound with Fn in LFAMF cause integrins pulling via Fn and resulted in activation of caspases cascade (Figure 2) we performed binding experiments with anti-Fn antibodies blocking the interaction of AS-14 with Fn (Figure 4). Three hours after treatment with AS-14-GMNPs in LFAMF activation of caspase 3/7 accurred in 35% of cells. Anti-Fn antibodies added to the cells prior the treatment occupied binding sites for AS-14-GMNPs and inhibited caspase cascade, while control anti-actin antibody did not (Figure 4A1).

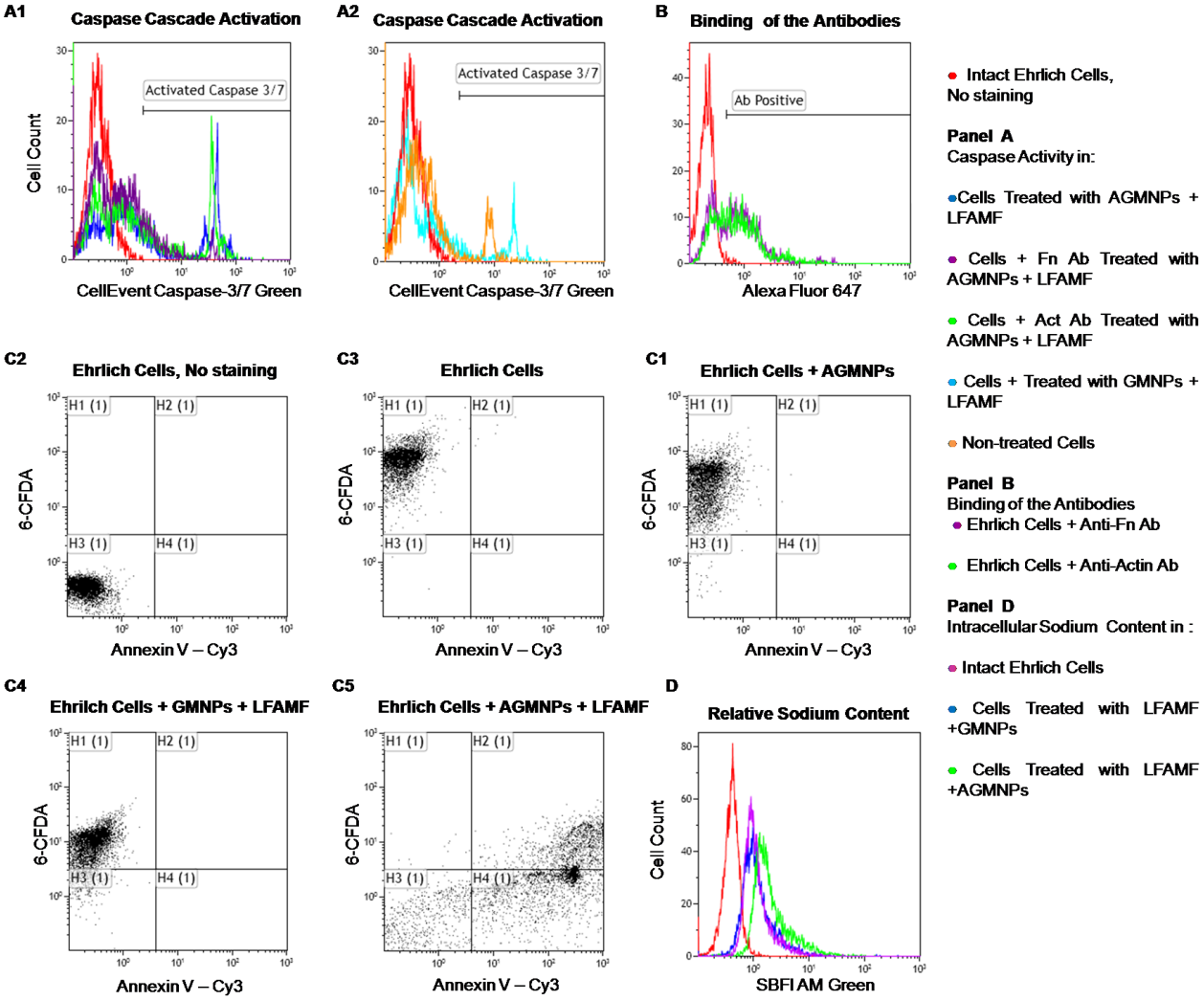

Figure 4. Mechanisms and efficacy of magnetodynamic nanotherapy *in vitro*. (A) Apoptosis estimated by caspase 3/7 activity;

(B) Apoptosis estimated by Annexin V-Cy3 labeling and 6-carboxyfluorescein diacetate (6-CFDA) staining of Ehrlich cells: (1)intact cells without staining; (2) viability of living cells; (3) cells 3 hours after exposure to LFAMF; (4) cells 3 hours after treatment with GMNPs and LFAMF; (5) cells 3 hours after treatment with AS-14-GMNPs (AGMNPs) and LFAMF. (B) Relative sodium content estimated by SBFI fluorescence intensity: the red curve corresponds to cells without staining, the purple - to untreated cells; the blue - to cells treated with GMNPs in LFAMF; and green to cells treated with AS-14-GMNPs in LFAMF.

In intact cells caspase 3/7 was activated in 11% of cells, treatment with GMNPs in LFAMF increased just fluorescence intensity, but not the number of apoptotic cells(Figure 4A2). We should note that these experiments have been performed in cell cultures which grew in suspension and thus express less extracellular Fn, than in solid tumor *in vivo* [16]. Anti-Fn antibodies bind only to 60% of cells (Figure 4B).

In cell cultures we demonstrate that AS-14-GMNPs in LFAMF- induced carcinoma cell death, which started with apoptotic phosphatidylserine translocation and followed by necrosis (Figure 4 C5). After the AS-14-GMNPs - LFAMF treatment, the majority of Annexin V positive cells were also CFDA negative (which indicates they were dead). Control experiments with AS-14-GMNPs alone without a magnetic field and GMNPs without aptamers with LFAMF treatment did not cause carcinoma cells death, but the cells accumulated less CFDA, and their membranes might have been slightly damaged. Moreover, the content of sodium cations in carcinoma cells increased after treatment with AS-14-GMNPs in LFAMF, suggesting necrosis (Figure 4D). Cell death can be caused by activation of different molecular pathways, including apoptosis, necrosis and autophagy, characterized by morphological and biochemical features [33]. Death processes are accompanied by a change in the cell volume due to a change in ion fluxes, especially sodium ions. Significant loss of sodium, potassium and chlorine ions are essential for activation of caspases and nucleases for apoptosis development [34]. In contrast, necrosis, is characterized by swelling of the cell because of increased sodium content. The lack of energy for Na^+/ K^+-ATPases in cellular necrosis causes swelling of cell followed by membrane rupture and inflammation.

***In Vivo* Antitumor Activity of Aptamer-Modified GMNPs in LFAMF**

In vivo antitumor efficacy of AS-14-GMNPs in LFAMF was evaluated using solid Ehrlich carcinoma in which the tumor was transplanted into the right leg of each mouse. The principal scheme of the experiment is presented in Figure 1 and described in details in Materials and Methods. Briefly, AS-14 modified GMNPs (1.6 μg kg^{-1}), free GMNPs, free AS-14 (0.4 mg kg^{-1}) and DPBS for control groups (7 animals in each) were injected intravenously, and after 30

minutes, LFAMF was applied for 10 minutes. The treatment procedures were repeated three times on alternate days starting on day 5 after tumor transplantation.

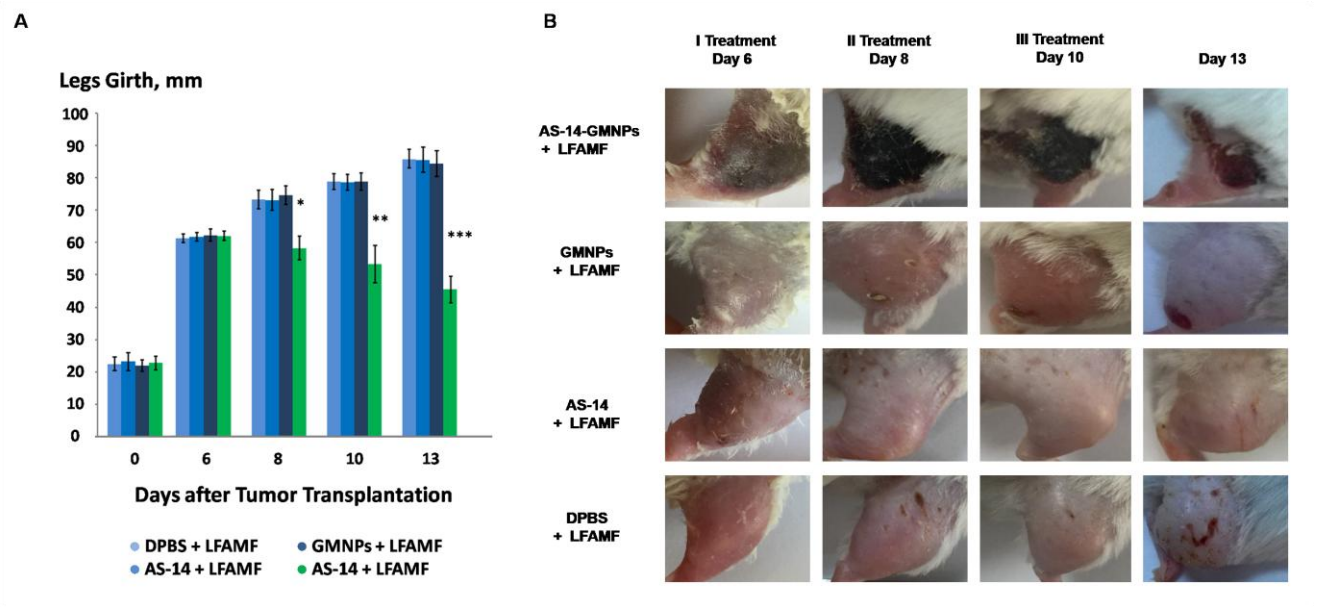

Figure 5. Efficacy of magnetodynamic nanotherapy *in vivo*. (A) Tumor size changes in the course of treatment (* $p<0.05$; ** $p<0.01$; *** $p<0.001$). (B) Imaging the tumor recovery after LFAMF treatment.

The efficacy of the treatment is presented in Figure 5A: tumor sizes were estimated by measuring legs girth regularly every day after treatment. The tumor size visually decreased after treatment with AS-14-GMNPs and LFAMF. On day 6, after the first treatment, a subcutaneous hemorrhage was observed in the leg with the tumor in each mouse injected with AS-14-GMNPs and exposed with LFAMF for 10 min (Figure 5B). On day 8,after a second treatment was performed on day 7, the tumor stopped growing and formed a crust, suggesting necrosis. After the third injection, on day 9, the wound began to heal. On day 13, the size of the crust reduced significantly and the skin around it almost fully recovered. Treatment with either GMNPs or AS-14 aptamer in LFAMF did not cause any reduction in tumor size. Injection of GMNPs with LFAMF exposure caused small inflammation of the tumor, which grew during the course of treatment, demonstrating the slight effect of GMNPs. We think that GMNPs themselves also cause tumor necrosis, but they are sufficiently less effective without the aptamer.

Mathematical simulations show that LFAMF does not cause hyperthermia itself or in the presence of GMNPs and AS-14-GMNPs. Therefore, the mechanical action of LFAMF on GMNPs linked through the aptamer with tumor cells can be explained as: Fn causes twitching of

the integrin β-domain which leads to its activation [24] and initiation of cell death by caspase cascade induction of primary apoptosis (Figure 2A) followed by sodium content increase (Figure 4B) and cancer cell necrosis (Figure 6 B10-B12). Considerable damage of the tumor *in vivo* and tumor size reduction by LFAMF occurred only when the GMNPs were aptamer modified and delivered to the tumor site (Figure 5). For non-specific accumulation of GMNPs in tumor, the effect was insufficient and may be a result of the 30-minute exposure time.

Aptamer-facilitated magnetodynamic nanotherapy at a low frequency (50 Hz) of alternating magnetic field did not cause local hyperthermia, which was demonstrated by mathematical simulations (Supporting Information).

Tissue Analyses after Magnetodynamic Nanotherapy

We identified that the reduction of tumor's size was due to the mechanical oscillations of AS-14-GMNPS in LFAMF. Five hours after the treatment with AS-14-GMNPs in LFAMF, caspase 3/7 were active in tumor cells (Figure 6A), whereas pure GMNPs or free AS-14 aptamer in LFAMF did not cause this effect.

Tumors did not respond to the control treatment with pure DPBS in LFAMF; cells stayed viable, tumors grew and destroyed muscle tissue, and the immune response was weak (Figure 6 B1-3).The control treatment with free aptamer AS-14 in DPBS and LFAMF did not show significant changes in tumor's structure; lymphocytic infiltration was still poor, swelling of the intermediate spaces was moderate, and muscle fibers were degenerative (Figure 6, B4-6).

Treatment with pure GMNPs caused partial necrosis of tumor tissues remaining in the form of "islands" (Figure 6, B7-B9). We observed tumor cells with cytoplasm vacuolization and signs of karyolysis, which is an irreversible result of the damaging effects of the treatment (Figure 6, B9). Inflammatory lymphocytic infiltration was expressed weakly around the tumor (Figure 6, B7-B9).

A significant therapeutic effect was observed in tumor tissues after treatment with AS-14-GMNPs in LFAMF (Figure 6 B9-B12). On the periphery of the large tumor necrosis areas remain small amounts of carcinoma cells, partly subjected to complete destruction or with irreversible changes: karyorrhexis, karyolysis, plasmorrhexis, these are the damaging effects of the treatment (Figure 6 B12). This treatment caused significant immune response as there was visible inflammatory infiltration of segmented leukocytes on the boundaries of necrotic areas. Swelling and destructive changes of tumor tissue microenvironment were also observed (Figure 6 B9-B12).

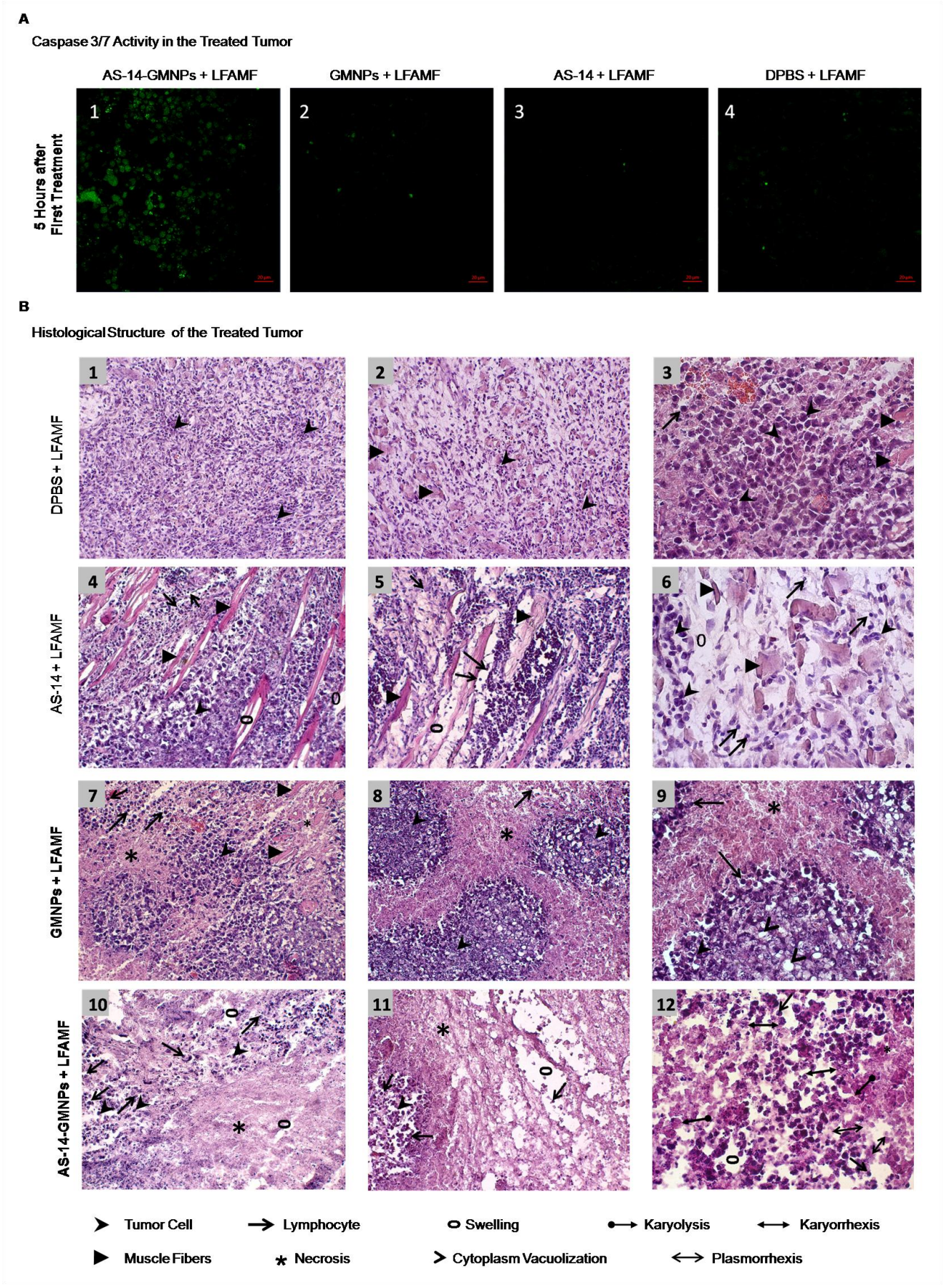
A
Caspase 3/7 Activity in the Treated Tumor
AS-14-GMNPs + LFAMF
GMNPs + LFAMF
AS-14 + LFAMF
DPBS + LFAMF
5 Hours after First Treatment
1
2
3
4
B
Histological Structure of the Treated Tumor
DPBS + LFAMF
AS-14 + LFAMF
GMNPs + LFAMF
AS-14-GMNPs + LFAMF
1
2
3
4
5
6
7
8
9
10
11
12
Tumor Cell
Lymphocyte
Swelling
Karyolysis
Karyorrhexis
Muscle Fibers
Necrosis
Cytoplasm Vacuolization
Plasmorrhexis

Figure 6. Tumor response to magnetodynamic nanotherapy.

(A) Caspase 3/7 activity in cancer cells from tissue sections of tumors harvested 5 hours after treatment.

(B) Histological structure of treated tumors. **B1-B3** – DPBS and LFAMF treated Ehrlich carcinoma has a solid structure and grows into the muscle tissue, composed of atypical cells with pleomorphic, hyperchromatic nuclei of different shapes and volume. No immune response: very rare lymphocytes. **B4-B6** – AS-14 and LFAMF treated carcinoma has moderate swelling of the intermediate spaces, poor lymphocytic infiltration and muscle fibers with degenerative changes. **B7-B9** – GMNPs and LFAMF treated carcinoma has scattered tumor necrosis with weakly expressed inflammatory infiltration, tumor tissue remains in the form of "islands" in which the majority of cancer cells are with cytoplasm vacuolization and signs of karyolysis. **B10-B12** – AS-14-GMNPs and LFAMF treated carcinoma has large tumor necrosis areas, swelling, destructive changes of tumor tissue microenvironment and inflammatory infiltration of segmented leukocytes. On the periphery remaining tumor cells are dead with karyorrhexis, karyolysis, plasmorrhexis. Magnification: (B1) ×100; (B2, B4, B5, B7, B8, B10, B11) × 200; (B3, B6, B9, B12) ×400.

Toxicity of aptamer-functionalized GMNPs was estimated by changes in blood serum biochemistry (Table 1). In addition it was made an attempt to estimate iron and gold distribution in different organs after intravenous injection of AS-14-GMNPs in DPBS (Figure S2). Electron microscopy revealed that a single dose of AS-14-GMNPs (1.6 μg kg^{-1}) is not sufficient for detection of iron and gold ions in the tumor, other organs and urine after 1, 5 and 24 hours (Figure S2). Cholesterol, serum alanine amino-transferase (ALT), alkaline phosphatase (ALP) and bilirubin are the standard parameters for drug hepatotoxicity evaluation [35]. ALT is involved in energy metabolism in liver, with lower enzymatic activities in other tissues, therefore it is considered as a specific biomarker of liver function. Total bilirubin, a product of hemoglobin degradation, is a marker of hepatobiliary injury and hemolysis [35]. ALP is associated with cell membrane's damage of hepatocytes [35]. In our experiments, 3 injections of AS-14-GMNPs administered to healthy male and female mice did not cause changes in these parameters compared to the control group treated with DPBS and was not dependent on gender. An inflammation and hydration status of the animals treated with nanoparticles was evaluated by total protein concentration [35], which did not significantly differ in the groups of male and

female mice treated with AS-14-GMNPs (Table 1). All tested parameters indicate that the treatment with AS-14-GMNPs is safe and does not cause hepatotoxic effects.

Table 1. Blood serum biochemistry parameters performed separately for male and female mice treated with AS-14-GMNPs in phosphate buffer (DPBS) or DPBS alone. All data are presented as the mean ± standard error of mean.

Sample	**Cholesterol, m mole L^{-1}**	**Total protein, g L^{-1}**	**Alanine amino-transferase, IU L^{-1}**	**Alkaline phosphatase, IU L^{-1}**	**Total bilirubin, µ mole L^{-1}**
AS-14-GMNPs					
Female (N=5)	1.45±0.01	50.75±3.32	18.40±3.67	214.30±74.81	5.67±0.38
Male (N=5)	1.56±0.48	55.97±6.21	31.90±13.17	254.87±122.29	6.05±0.21
DPBS					
Female (N=5)	2.30±0.28	53.90±1.27	13.55±4.78	177.67±27.13	6.25±0.70
Male (N=5)	2.32±0.26	55.90±2.76	20.93±6.9	251.40±71.13	6.20±0.53

Conclusion

Our study demonstrates the therapeutic effect of magnetodynamic nanotherapy guided by cell specific aptamers on cancer. Further investigations need to be performed to better understand the mechanism of action of AS-14-GMNPs in LFAMF and overall toxicity of AS-14-GMNPs and LFAMF on normal tissues. Promising opportunities for effective applications of the proposed method are based on using aptamer-functionalized gold- coated magnetic nanoparticles for targeted tumor treatment in a low frequency alternating magnetic field, which selectively destroys cancer cells without affecting non-malignant adjacent cells and tissues.

Acknowledgements

The authors are grateful to George Y. Vorogeikin, Yuri I. Vorogeikin and "OKB ART" for the infrared imaging. Andrey Barinov and "OPTEC Group"for help with 3D laser scanning imaging. Microscopic analyses using Carl Zeiss LSM 800 were done in the "Center for bioassay, nanotechnology and nanomaterials safety" ("Biotest-Nano") (Multiple-Access Center, Tomsk State University, Tomsk, Russia). Toxicity studies have been performed in Multiple-Access Center, Central Scientific Research Laboratory in Krasnoyarsk State Medical University named after prof. V.F. Voino-Yasenecky. This work was supported by the Russian Scientific Fund (grant #14-15-00805).

Competing Interests

The authors declare no competing financial interests.

References

1. El-Sayed M. Small is different: Shape-, size-, and composition-dependent properties of some colloidal semiconductor nanocrystals. Accounts of Chemical Research. 2004; 37: 326-33.
2. Huang X, Jain P, El-Sayed I, El-Sayed M. Gold nanoparticles: interesting optical properties and recent applications in cancer diagnostic and therapy. Nanomedicine : nanotechnology, biology, and medicine. 2007; 2: 681-93.
3. Davis M, Chen Z, Shin D. Nanoparticle therapeutics: an emerging treatment modality for cancer. Nature Reviews Drug Discovery. 2008; 7: 771-82.
4. Liu Q, Jin C, Wang Y, Fang X, Zhang X, Chen Z, et al. Aptamer-conjugated nanomaterials for specific cancer cell recognition and targeted cancer therapy. Npg Asia Materials. 2014; 6.
5. Malik M, O'Toole M, Casson L, Thomas S, Bardi G, Reyes-Reyes E, et al. AS1411-conjugated gold nanospheres and their potential for breast cancer therapy. Oncotarget. 2015; 6: 22270-81.
6. Banerjee R, Katsenovich Y, Lagos L, McIintosh M, Zhang X, Li C. Nanomedicine: Magnetic Nanoparticles and their Biomedical Applications. Current Medicinal Chemistry. 2010; 17: 3120-41.
7. Dreaden E, Alkilany A, Huang X, Murphy C, El-Sayed M. The golden age: gold nanoparticles for biomedicine. Chemical Society reviews. 2012; 41: 2740-79.
8. Wu P, Gao Y, Lu Y, Zhang H, Cai C. High specific detection and near-infrared photothermal therapy of lung cancer cells with high SERS active aptamer-silver-gold shell-core nanostructures. Analyst. 2013; 138: 6501-10.
9. Gu F, Karnik R, Wang A, Alexis F, Levy-Nissenbaum E, Hong S, et al. Targeted nanoparticles for cancer therapy. Nano today. 2007; 2: 14-21.
10. Bugaj AM. Targeted photodynamic therapy - a promising strategy of tumor treatment. Photoch Photobio Sci. 2011; 10: 1097-109.
11. Luo YL, Shiao YS, Huang YF. Release of Photoactivatable Drugs from Plasmonic Nanoparticles for Targeted Cancer Therapy. Acs Nano. 2011; 5: 7796-804.
12. Hu XG, Gao XH. Multilayer coating of gold nanorods for combined stability and biocompatibility. Physical Chemistry Chemical Physics. 2011; 13: 10028-35.
13. Shi H, Ye XS, He XX, Wang KM, Cui WS, He DG, et al. Au@Ag/Au nanoparticles assembled with activatable aptamer probes as smart "nano-doctors" for image-guided cancer thermotherapy. Nanoscale. 2014; 6: 8754-61.
14. Huang YF, Sefah K, Bamrungsap S, Chang HT, Tan W. Selective Photothermal Therapy for Mixed Cancer Cells Using Aptamer-Conjugated Nanorods. Langmuir. 2008; 24: 11860-5.
15. Kolovskaya OS, Zamay TN, Zamay AS, Glazyrin YE, Spivak EA, Zubkova OA, et al. DNA-Aptamer/Protein Interaction as a Reason of Apoptosis and Proliferation Stop in Ehrlich Ascites Carcinoma Cells. Biologicheskie Membrany. 2013; 30: 398-411.
16. Zardi L, Cecconi C, Barbieri O, Carnemolla B, Picca M, Santi L. Concentration of fibronectin in plasma of tumor-bearing mice and synthesis by Ehrlich ascites tumor cells. Cancer Research. 1979; 39: 3774-9.
17. Fernandez-Garcia B, Eiro N, Marin L, Gonzalez-Reyes S, Gonzalez L, Lamelas M, et al. Expression and prognostic significance of fibronectin and matrix metalloproteases in breast cancer metastasis. Histopathology. 2014; 64: 512-22.
18. Pankov R, Yamada K. Fibronectin at a glance. Journal of cell science. 2002; 115: 3861-3.
19. Ritzenthaler J, Han S, Roman J. Stimulation of lung carcinoma cell growth by fibronectin-integrin signalling. Molecular bioSystems. 2008; 4: 1160-9.

20. Hynes R. The emergence of integrins: a personal and historical perspective. Matrix Biology. 2004; 23: 333-40.
21. Campbell I, Humphries M. Integrin Structure, Activation, and Interactions. Cold Spring Harbor perspectives in biology. 2011; 3.
22. Luo B, Carman C, Takagi J, Springer T. Disrupting integrin transmembrane domain heterodimerization increases ligand binding affinity, not valency or clustering. P Natl Acad Sci USA. 2005; 102: 3679-84.
23. Takagi J, Springer T. Integrin activation and structural rearrangement. Immunological reviews. 2002; 186: 141-63.
24. Puklin-Faucher E, Gao M, Schulten K, Vogel V. How the headpiece hinge angle is opened: new insights into the dynamics of integrin activation. J Cell Biol. 2006; 175: 349-60.
25. Puklin-Faucher E, Sheetz M. The mechanical integrin cycle. Journal of cell science. 2009; 122: 179-86.
26. Puklin-Faucher E, Vogel V. Integrin Activation Dynamics between the RGD-binding Site and the Headpiece Hinge. Journal of Biological Chemistry. 2009; 284: 36557-68.
27. Danen E. Integrin Proteomes Reveal a New Guide for Cell Motility. Science signaling. 2009; 2.
28. Danen E, Ruiter D, Vanmuijen G. Mechanisms of Melanoma Cell-Adhesion to Fibronectin. Biochemical Society transactions. 1995; 23: S403-S.
29. Danen E, Sonnenberg A. Integrins in regulation of tissue development and function (vol 200, pg 471, 2003). Journal of Pathology. 2003; 201: 632-41.
30. Danen E, Sonneveld P, Sonnenberg A, Yamada K. Dual stimulation of Ras/Mitogen-activated protein kinase and RhoA by cell adhesion to fibronectin supports growth factor-stimulated cell cycle progression. J Cell Biol. 2000; 151: 1413-22.
31. Danen E, van Rheenen J, Franken W, Huveneers S, Sonneveld P, Jalink K, et al. Integrins control motile strategy through a Rho-cofilin pathway. J Cell Biol. 2005; 169: 515-26.
32. Zhang Y, Chen M, Venugopal S, Zhou Y, Xiang W, Li Y, et al. Isthmin exerts pro-survival and death-promoting effect on endothelial cells through alphavbeta5 integrin depending on its physical state. Cell death & disease. 2011; 2.
33. Bortner C, Cidlowski J. Ion channels and apoptosis in cancer. Philosophical Transactions of the Royal Society B-Biological Sciences. 2014; 369.
34. Bortner C, Cidlowski J. Uncoupling cell shrinkage from apoptosis reveals that Na+ influx is required for volume loss during programmed cell death. Journal of Biological Chemistry. 2003; 278: 39176-84.
35. A. Wallace Hayes, Claire L. Kruger. Hayes' Principles and Methods of Toxicology, Sixth Edition. 2014; 824.

Supporting Information

In Vivo Cancer Cells Elimination Guided by Aptamer-Functionalized Gold-Coated Magnetic Nanoparticles and Controlled with Low Frequency Alternating Magnetic Field

Irina V. Belyanina[2,3], Tatiana N. Zamay[2,3], Galina S. Zamay[1,2], Sergey S. Zamay[1], Olga S. Kolovskaya[1,2], Tatiana I. Ivanchenko[2], Valery V. Denisenko[5,3], Andrey K. Kirichenko[2], Yury E. Glazyrin[2], Irina V. Garanzha[2,3], Valentina V. Grigorieva[2,3], Alexandr V. Shabanov[1], Dmitry V. Veprintsev[1,2], Alexey E. Sokolov[1,3], Vladimir M. Sadovskii[5,3], Ana Gargaun[4], Maxim V. Berezovski[4], Anna S. Kichkailo[1,2]

[1]*Federal Research Center, KSC Siberian branch of Russian Academy of Science, Krasnoyarsk, Russia*

[2]*Krasnoyarsk State Medical University named after Professor V. F. Voyno-Yasenetsky, Krasnoyarsk, Russia*

[3]*Siberian Federal University, Krasnoyarsk, Russia*

[4]*University of Ottawa, Department of Chemistry and Biomolecular Sciences, Ottawa, Ontario Canada*

[5]*Institute of Computational Modeling RAS SB, Krasnoyarsk, Russia*

Corresponding authors: Anna S. Kichkailo, azamay@krasgmu.ru

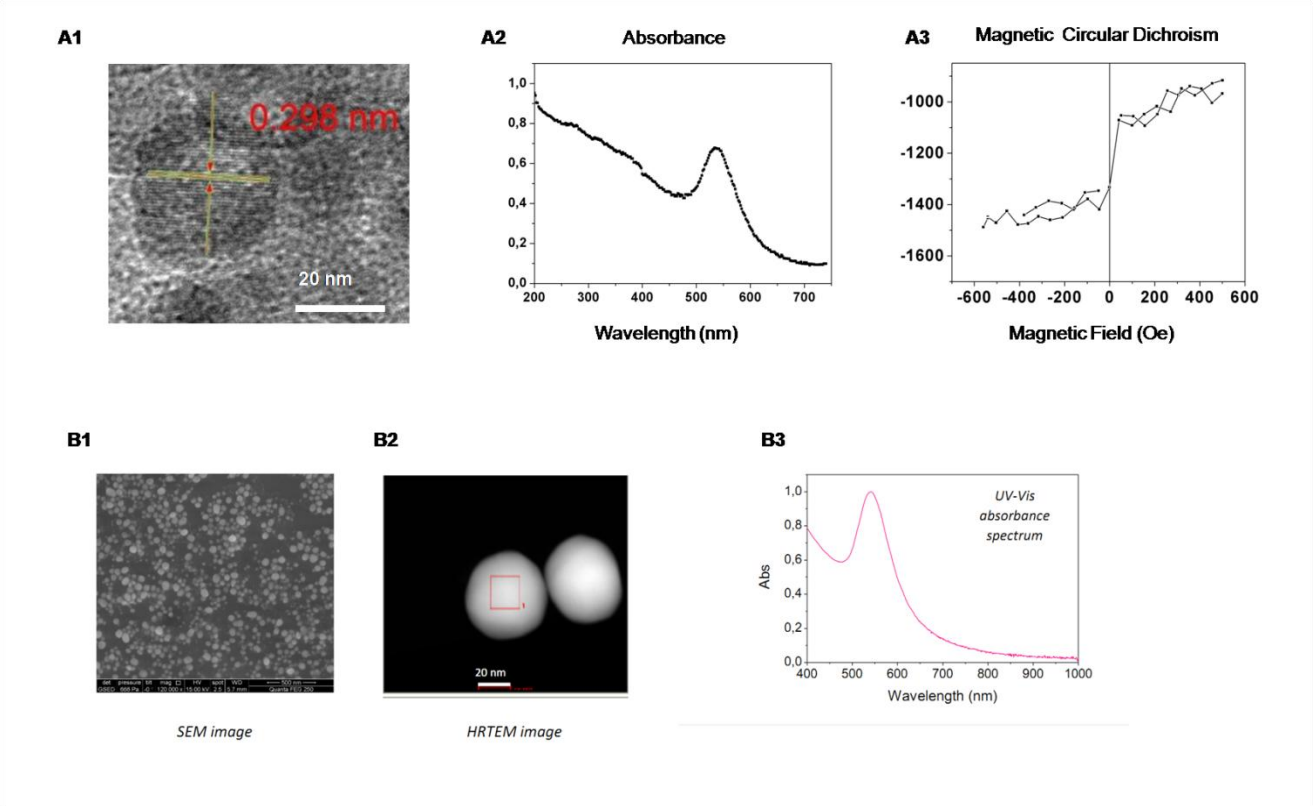

Figure S1. Properties of magnetic nanoparticles NITmagoldCit of 50nm from Nanoimmunotech, Spain.

(A) Scanning electron microscopy of aptamer modified GMNPs (1); absorbance (2); magnetic circular dichroism before the experiment (3).

(B) Scanning electron microscopy (1); high-resolution transmission electron microscopy (2); absorbance from product datasheet.

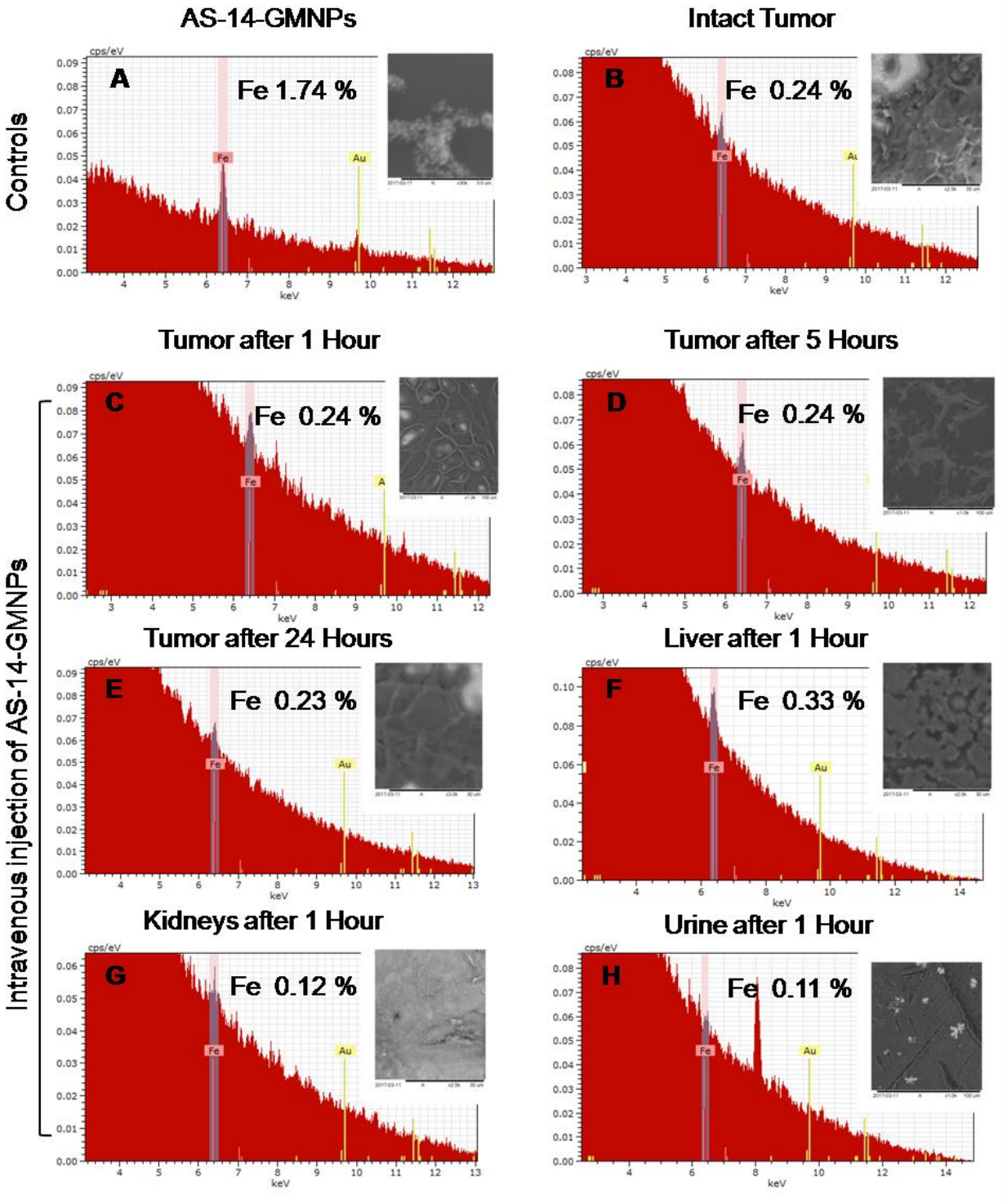
Controls
Intravenous injection of AS-14-GMNPs
AS-14-GMNPs
A
Fe 1.74 %
Intact Tumor
B
Fe 0.24 %
Tumor after 1 Hour
C
Fe 0.24 %
Tumor after 5 Hours
D
Fe 0.24 %
Tumor after 24 Hours
E
Fe 0.23 %
Liver after 1 Hour
F
Fe 0.33 %
Kidneys after 1 Hour
G
Fe 0.12 %
Urine after 1 Hour
H
Fe 0.11 %
cps/eV
keV
Fe
Au

Figure S2. Distribution of iron and gold ions in organs after intravenous injection of AS-14GMNPs in 100 μL DPBS (1.6 μg kg^{-1}) determined by electron microscopy (EM). Spectral analyses of iron and gold content in AS-14GMNPs (A); thin section of the intact tumor tissue (B); tumor 1 (C), 5 (D) and 24 (E) hours (C) after intravenous injection of AS-14GMNPs; liver (F), kidneys (G), and urine (H) 1 hour after injection of AS-14GMNPs. Inserts - contrast EM of the correspondent sample.

The mechanical action of the magnetic particles on cells

If a magnetite particle has a spherical shape of radius R_p, then its magnetic moment in a uniform external magnetic field $\vec{H}_0$ equals to

$$d = 4\pi R_p^3 \frac{\mu - 1}{\mu + 2} H_0,$$

where μ - relative magnetic permeability, which value for magnetite is close to 5 according to the data [3]. This formula follows from the known exact solution for the problem of magnetization of a homogeneous ball [2]. Magnetic moment of a ball is directed along the field $\vec{H}_0$, and therefore no torque appears. Any field inhomogeneity leads to magnetophoresis that we do not consider here.

Shape of our magnetic particles is substantially different from a ball. In such a case, the magnetic moment is large, if the body is elongated along the field $\vec{H}_0$, and small for another orientation. For bodies of particular shapes, these parameters can be calculated. We assume that our particle is a prolate ellipsoid of revolution, and the long half-axis $a = 12$ nm is twice longer than the short ones $b = 6$ nm. The exact solution for the problem of magnetization of the ellipsoid is known [2]. For μ = 5 it gives the magnetic moments in the direction of elongation and normal one

$d_{1,2} \approx (1 \pm 0.17) 8ab^2 H_{1,2}$.

If there is an angle ϑ between the magnetic field $\vec{H}_0$and the direction of elongation of the body, the magnetic moment is not parallel to the field. The projections of the moment on the field H_0 and normal to it equal $d_1 \cos\vartheta$ and $d_2 \sin\vartheta$. Hence, there is a torque

$$N = (d_1 - d_2)\mu_0 H_0 \sin(\vartheta)\cos(\vartheta) \approx 1.4\mu_0 ab^2 H_0^2 \sin(2\vartheta),$$

where μ_0 - magnetic permeability. If the magnetic field strength $H_0 = 8$ kA/m, which corresponds to 100 Oe, the torque depending on the angle ϑ can reach $0.5 \cdot 10^{-22}$ N·m.

Figure 3 is a diagram of the mechanical interaction of the magnetic particle with the cell. We use superparamagnetic particles which are covered by a thick layer of gold, so that from the outside they look like balls of radius $R_p = 25$ nm. Their surface is covered with aptamers which cling to fibronectin filaments located in the intercellular space. These filaments are attached at their ends to integrins located in cell membranes. We approximately simulate the filaments as inextensible ones and we consider integrins as solid cylinders of radius $R = 2$ nm.

When under the influence of the magnetic field the particle is rotated clockwise, as shown in Figure 3, it pulls the left filament up and pulls the right one down. The left filament above the particle can be bent, and therefore does not transmit efforts at its upper end. The lower part of this filament pulls integrin with the force $\vec{F}$. Similarly, the right filament does not act on the integrin shown in Figure 3, but pulls the other integrin, located somewhere above the drawing area.

For evaluation of the elastic forces generated by pulling integrin to the height h, we approximately assume that all the elastic forces are determined by deformation of the membrane. According to [1] the mammalian cell membranes in the normal state are stretched so that the order of magnitude of the tension $\tau = 10^{-5}$ N/m. It may be noted that this tension of the membrane is balanced by the pressure inside the cells increased by $\Delta P = 2\tau / R_c$ as compared with the pressure in surrounding environment. For the cells with radius $R_c = 10\,\mu$m, this difference $\Delta P \approx 2$ P.

We are interested in the phenomenon with a scale much smaller than the radius of the cell R_c. So we neglect the curvature of the membrane. We consider a thin membrane, and we suppose that it is fixed at the circle of some large radius R_∞. In our model the integrin looks like a solid circle of radius R centered at the same point as the center of the selected circle of the membrane.

This object is rotationally symmetric. Hence, we use the polar coordinates r, φ of the points in the plane of the non-deformed membrane. Points do no move in direction of φ because of the symmetry. For small strains the displacement in direction of r has a higher order of smallness than the deflection in the direction normal to the membrane. The latter is denoted as $w(r)$. Therefore, the displacement of the membrane points is described by one function $w(r)$. The following boundary conditions correspond to the rise to the height h at the circle $r = R$ and zero displacement at $r = R_\infty$

$$w(R) = h, \quad w(R_\infty) = 0. \qquad (1)$$

The membrane takes such a form that the elastic energy J reaches a minimum. In our case of axial symmetry in accordance with [4], we have

$$J = \pi\tau \int_R^{R_\infty} \left(\frac{dw}{dr} \right)^2 r\,dr .$$

The condition of its minimum is the equation

$$\frac{1}{r}\frac{d}{dr}\left(r\frac{dw}{dr} \right) = 0 .$$

Its solution is the function

$$w(r) = A\ln(r / B),$$

where A, B - arbitrary constants. Their values can be found from the boundary conditions (1). The result is

$$w(r)=h\ln(R_\infty / \mathrm{r})/\ln(R_\infty / R). \qquad (2)$$

The graph of this solution is shown in qualitative manner in Figure 3.

Such a membrane is inclined relative to the plane at the angle β, such that

$$tg(\beta(r))=\frac{dw(r)}{dr}=\frac{-h}{\ln(R_\infty / \mathrm{R})}\frac{1}{r}. \qquad (3)$$

This slope on the border with the solid circle defines the force with which the membrane draws the circle dawn in the vertical direction

$$F=2\pi R\tau\cdot\sin\beta\approx 2\pi\tau h/\ln(R_\infty / R). \qquad (4)$$

The formula is simplified for small angle β, when $tg\,\beta\approx\beta\approx\sin\beta$. This expression contains one parameter R_∞, whose value we have identified only by the inequalities

$$R_c \gg R_\infty \gg R.$$

The uncertainty of R_∞ can be solved only within a more general model that takes into account spherical membrane. We do not do this, since the logarithm $\ln(R_\infty / R)$ in (2-4) is only slight varied when R_∞ changes in a wide range. Take the seemingly reasonable average value $R_\infty=\sqrt{R_c R}\approx 150$ nm when $\ln(R_\infty / R)\approx 4$. Expression (4) reduces to

$$F\approx 1.5\tau h. \qquad (5)$$

The maximum value of torque $N=0.5\cdot 10^{-22}$ N·m due to the magnetic field acting on the magnetic particle was obtained above. It is easy to show that since we use low frequencies, the inertia during the rotation of the particle can be neglected. The friction of the surrounding liquid is more important, but the friction torque is alsoa few orders of magnitude smaller than the torque N. Therefore, the pair of the elastic force (5) and having the same module elastic force applied to the right-hand filament in Figure 3, balances the torque N. It gives the equality

$$N\approx 3\tau h R_p,$$

that permits to evaluatethe height to which integrins can be drawn by the magnetite particles which we use, $h\approx 0.07$ nm. Possibly, the angle $\beta(R)\approx 0.5^0$ of rotation of the membrane in the place of its attachment to the integrin (3) is of value. The force (5), that pull the integrin from the membrane can be up to $F\approx 10^{-15}$ N. It can be mentioned that the magnetic particle rotates h/R_p angle that is of about 0.15^0 when $h=0.07$ nm.

Note that these values of h, F are obtained only for the magnetic particles oriented in a certain way with respect to the direction of the external magnetic field $\vec{H}_0$. Since the particles when attached to the cells are randomly oriented, the specified parameter values ought to be reduced several times to estimate the average impact on a cell.

The obtained limit values could be achieved when varying over time magnetic field $\vec{H}_0$ has amplitude value, that occurs twice during the period. The frequency is 50 Hz in our experiments. When the magnetic field $\vec{H}_0$ is reversed, the magnetic moment of each magnetite particle does the same. The torque keeps sign since it equals to their vector product. Consequently, during

both half cycles the particle rotates in the same direction when the field strength increases, and returns to its free position when the field is weakened. Therefore, during 0.01 sec integrin is pulled out of the cell to a height about 0.07 nm and returns to its original position. Perhaps, just these twitches with frequency 100 Hz damage cells in our experiments, whereas the stationary membrane deformations of the same scale could be not so effective.

Heating

Let us show that the thermal energy released in magnetic particles is distributed throughout the liquid. In our experiments, the particles have a concentration of the order of $10^{14}\,\mathrm{m}^{-3}$, so the distance between adjacent particles $L \simeq 2\cdot 10^{-5}$ m. By the heat conduction equation typical time of heat propagation for the distance L is assessed as

$$\tau \simeq \frac{C}{\lambda}\cdot L^2,$$

where C - heat capacity λ - thermal conductivity. For water, $C = 4.2\cdot 10^6$ J/(m^{3}K), $\lambda = 0.6$ W/(m$\cdot$K). We get the characteristic time $\tau \simeq 0.003$ seconds. Such a small τ ensures uniform heating throughout the liquid and particles, not only for total time of the experiment $t = 10$ minutes, but even during the period of the magnetic field variation that equals $1/f =$ 0.02 seconds.

First, we study the heating of the metal particles in an alternating magnetic field.

In our experiments, we use an alternating magnetic field with strength of about 100 Oe or 8 kA/m, that corresponds to the magnetic induction $B = 0.01$ T. This field varies with time at a frequency $f = 50$ Hz.

Living cells and magnetic particles can be in different liquids. All of these liquids have salinity not exceeding seawater salinity. Therefore, to estimate maximum effect, consider seawater which conductivity is $\sigma_l = 3$ S/m. The main part of the used magnetic particles takes gold which conductivity is $\sigma_p = 0.5 \cdot 10^7$S/m.

The nature of the influence of a substance on the alternating magnetic field is determined by such a parameter as the thickness of the skin layer $\delta = 1/\sqrt{\pi\sigma\mu_0 f}$, and $\delta_l = 40$ m for the liquid and $\delta_p = 1$ cm for gold. Here μ_0 is magnetic permeability of vacuum. Because these parameters are many orders of magnitude greater than the characteristic size of the region occupied by the liquid, and the size of the particles, respectively, the magnetic field freely permeates without being distorted into the liquid and into the particles.

By virtue of the law of electromagnetic induction the variation of the magnetic field creates a vortex electric field $\vec{E}$ which satisfy the equation

$$\oint \vec{E} d\vec{l} = -\frac{\partial}{\partial t}\int \vec{B} d\vec{s}, \qquad (6)$$

where the integration in the left side is made over an arbitrary closed circuit, and in the right side - over the surface bounded by this circuit, t - time.

To simplify estimates, assume that liquid occupies a region which is symmetric with respect to rotation about the same axis as that of the solenoid which generates a magnetic field. The magnetic field is assumed homogeneous, and its induction is defined as $B\cos(2\pi ft)$. Then the electric field is also axially symmetric and has only an azimuthal component $-E\sin(2\pi ft)$, and the integration in (6) for a circle of radius r is simple. Get

$$-2\pi rE\sin(2\pi ft) = \frac{\partial}{\partial t}(B\cos(2\pi ft)\,\pi r^2).$$

We express E, and for all points of the fluid at a distance of less than 5 mm from the axis, we obtain the estimate

$$E = r\pi fB < 0.01 \text{ V/m}.$$

The electric current produced by this field has a density $j = \sigma_l E < 0.03$ A/m^2, and is accompanied by Joule dissipation which density equals $jE = \sigma_l E^2 < 3\cdot 10^{-4}$ W/m^3. This energy heats the liquid. The temperature rises from the initial value T_0 to

$$T = T_0 + t\cdot jE/C,$$

after the time t. C - heat capacity per unit volume. For water, $C = 4.2\cdot 10^6$ J/(K·m^3). For $t = 10$ minutes the temperature is increased by

$$T - T_0 < 5\cdot 10^{-8}\text{K}, \qquad (7)$$

that is negligible.

Now consider the heating of the gold ball, placed in the liquid. Since the radius of the ball, $R = 25$ nm, is much smaller than the distance between the balls, each ball can be considered separately, as being in an infinite domain with a uniform electric field with strength $\vec{E}$, which module is E.

We know the exact solution of this problem of electrical conductivity. The electric potential V in spherical coordinates r, ϑ, φ, with the axis $\vartheta = 0$ directed along $\vec{E}$, has the form

$$V = \begin{cases} -E_p r\cos\vartheta\,, & r < R \\ (A/r^2 - Er)\cos\vartheta\,, & r > R, \end{cases}$$

where the constants

$$A = ER^3\big(\sigma_p/\sigma_l + 1\big)/\big(\sigma_p/\sigma_l + 2\big),$$

$$E_p = 3E/\big(\sigma_p/\sigma_l + 2\big).$$

Linear dependence of the electric potential on the coordinate $z = r\cos\vartheta$ inside the ball means a uniform electric field with strength $E_p \approx 3E\sigma_l/\sigma_p$, because $\sigma_p/\sigma_l \gg 1$. Accordingly, the density of Joule dissipation inside the ball equals $\sigma_p E_p^2 \approx 9E^2\sigma_l/\sigma_p$, that differs $9\sigma_l/\sigma_p \ll 1$ times from dissipation in the liquid. The electric field strength in the vicinity of the ball as compared to E do not increase more than threefold, and returns to the value E with the distance from the ball.

Accordingly, the density of Joule dissipation increases only in a small neighborhood of the ball and no more than 9 times.

Thus, the ball with high electric conductivity increases heating of some surrounding liquid, while the ball itself heats much less than liquid would be heated without it. The heating is negligible in view of the inequality (7).

One more important mechanism of energy transfer from the magnetic field to the medium is the work done by rotating particles.

Upon rotation of the particle the magnetic field does work $A = N\,\delta\varphi$, where $\delta\varphi$ - the angle of rotation, N - torque. Above, we obtain an estimate $\delta\varphi \simeq 0.15^0 \simeq 0.003$ radians. It was used the assumption that fibronectin filaments may be regarded as inextensible ones. If, on the contrary, they are easily stretched, they have virtually no influence on the rotation of the particles, which would turn to the ellipsoid orientation along the magnetic field, therefore, $\delta\varphi$ may be of the order of one radian. Of course, in such a case the cell membrane is not deformed, and all resistance would be determined by a rotation viscosity of the liquid. To evaluate the work from above, we use the limit $\delta\varphi \simeq 1$ radian and obtain $A < N$. All this work is ultimately converted into heat. The particle has a volume much smaller volume of fluid surrounding it, and this thermal energy is rapidly distributed throughout the liquid. Therefore, the law of conservation of energy can be written as

$$C L^3 (T - T_0) = 2 f t A,$$

where the frequency f is doubled, as the turns occur twice in the period of the field variation, and each time the magnetic field does the work A. Substituting the above estimates $A < N$, $N = 0.5 \cdot 10^{-22}$ N·m, obtains an estimate of the temperature change

$$T - T_0 < \frac{2 f N}{C L^3} t \simeq 10^{-10}\ K\ . \qquad (8)$$

This heating is negligible.

Another heating mechanism is associated with losses in reverses of magnetization of particles. Hysteresis for the magnetite particles is so small that it is difficult to find the magnetization curves at the amplitude of the field $H_0 = 100$ Oe = 8 kA/m, as in our experiments. Upper estimate can be obtained using the curves plotted in [3] at the amplitude of the field around 3000 Oe. The difference per unit mass of the magnetization with increasing and decreasing field is of about 2 A·m/kg. For magnetic density of about 5000 kg/m^3, we get $\delta M = 10^4$ A/m. The hysteresis loop at low fields is definitely inside the loop obtained for large amplitude of the field, so its area

$$-\oint \vec{H} d\vec{M} = \oint \vec{M} d\vec{H} < 2 \vec{H}_0 \delta \vec{M}\ .$$

The heat release in each cycle of magnetization is obtained by multiplying by the volume of the magnet and by μ_0. We get energy

$$2\mu_0 \frac{4}{3}\pi ab^2 H_0 \delta M \simeq 4\cdot 10^{-22}\,\text{J}.$$

Since this energy is four times more than the energy dissipation of turning particles, heating also increases four times compared with (8), and hence it is also negligible. This is consistent with the statement [3] about the possibility to neglect by hysteresis.

The same article [3] also considered other mechanisms of medium heating due to exposure to a magnetic field, such as Néel and Brownian relaxations. We do not analyze them in detail, and use the obtained theoretical estimates in [3], backed up by their experimental data. For magnetite particles with similar particle sizes in the field $H_0 = 150$ Oe varying with frequency 100 kHz the total heat release does not exceed 50 kW/kg. Their data demonstrate a linear dependence of the frequency and quadratic dependence of H_0. Under our $f = 50$ Hz and $H_0 = 100$ Oe we receive less than 10 W/kg. The mass of our magnetic particle is of about 10^{-20} kg. Thus, the released thermal energy is of about 10^{-19} W or 10^{-21} J per half-cycle of the magnetic field variation.

Since this energy is 10 times more than the energy dissipation of turning particles, heating is also increased 10 times as compared with (8), and hence it is also negligible.

Absence of heating in our experiments, as opposed to experiments on hyperthermia, is due to a lower magnetic field frequency and the smallness of the concentrations of magnetite particles. Our values of these parameters are three and eight orders of magnitude, respectively, less compared with the parameters used in [3] when a substantial heating was observed, up to 10 K per hour.

Thus, the alternating magnetic field has no thermal effect on the cells in our experiments.

1. Gauthier N., T. Masters, and M. Sheetz. Mechanical feedback between membrane tension and dynamics. Trends Cell Biol. 2012; 22: 527–35.

2. Landau L.D., E.M. Lifshitz. Theoretical physics. V. 8. Electrodynamics of Continuous Media. Moscow Nauka. 1982; 620.

3. Shubitidze F., K. Kekalo, R. Stigliano, and I. Baker. Magnetic nanoparticles with high specific absorption rate of electromagnetic energy at low field strength for hyperthermia therapy. Journal of Applied Physics. 2015; 117: 094302.doi: 10.1063/1.4907915.

4. Washizu K. Variational Methods in Elasticity & Plasticity. Oxford-New York, Pergamon Press. 1982; 630.

TOC figure

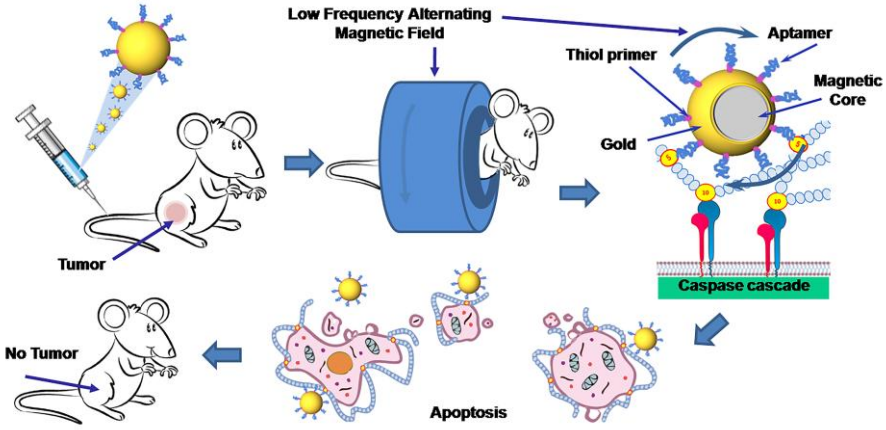
Low Frequency Alternating
Magnetic Field
Thiol primer
Aptamer
Magnetic
Core
Gold
Tumor
Caspase cascade
No Tumor
Apoptosis